Proceedings of the ASME 2013 32nd International Conference on Ocean, Offshore and Arctic Engineering
OMAE2013
June 9-14, 2013, Nantes, France

OMAE2013-10911

DRAFT: 2-D URANS VS. EXPERIMENTS OF FLOW INDUCED MOTIONS OF MULTIPLE CIRCULAR CYLINDERS WITH PASSIVE TURBULENCE CONTROL

Lin Ding
linding@cqu.edu.cn
College of Power Engineering
Chongqing University, Chongqing, China

Yang Chen
chanyang@umich.edu
Dept. of Naval Architecture & Marine Engineering
University of Michigan Ann Arbor, MI, USA

Eun Soo Kim
bblwith@umich.edu
Dept. of Mechanical Engineering
University of Michigan Ann Arbor, MI, USA

Michael M. Bernitsas[1]
michaelb@umich.edu
Dept. of Naval Architecture & Marine Engineering
University of Michigan Ann Arbor, MI, USA

ABSTRACT

Two-dimensional URANS equations are used to simulate the flow and body kinematics of the transverse motion of spring-mounted circular cylinders. Passive Turbulence Control (PTC) in the form of selectively distributed surface roughness is used to alter the cylinder Flow Induced Motion (FIM). PTC was proven in the past to make CFD and experiments compatible for a single cylinder in FIM for Reynolds number up to 135,000. Simulation is performed using a solver based on the open-source CFD tool OpenFOAM. Channel, oscillators, flow, cylinder, and PTC parameters match those of tests conducted in the Marine Renewable Energy Laboratory (MRELab) of the University of Michigan for $30{,}000<Re<150{,}000$. Four sets of simulations with 1/2/3/4 cylinders in tandem are investigated. Center-to-center distance between two cylinders is fixed at 2.5 diameters. Simulations are conducted at two Reynolds numbers one corresponding to VIV and one to transition from VIV to galloping. The results are compared with experimental data measured in the MRELab. Vortex patterns, amplitude and frequency ratio predicted by CFD for PTC-cylinders match well with experimental measurements at such high Reynolds numbers. The developed CFD tool can be useful in understanding the FIM (VIV, galloping) of multiple cylinders in tandem.

1. INTRODUCTION

Recent developments, in the Marine Renewable Energy Laboratory (MRELab) at the University of Michigan on passive turbulence control (PTC) of elastically mounted rigid circular-cylinders have improved dramatically the hydrodynamics of the VIVACE (Vortex Induced Vibration for Aquatic Clean Energy) Converter. The *PTC-to-FIM Map* is a powerful tool altering the Flow Induced Motions (FIM) of a cylinder on springs. It can be used to enhance or suppress FIM [3]. Enhancement is used in harnessing hydrokinetic energy [1-5, 7-13]. VIVACE is a hydrokinetic-power-generating device invented by Bernitsas and Raghavan [1,2,12,13] and is being developed in the MRELab [7-13]. It harnesses hydrokinetic energy from even slow ocean/river currents. The lowest speed achieved in the lab is 0.35m/s=0.68knots [9,10]. The upper limit has not been determined as yet. A single VIVACE module is simple and consists of a circular cylinder mounted on springs with a PTO (Power Take Off) system.

Contrary to the traditional engineering challenge of reducing FIM – mostly Vortex Induced Vibration (VIV) and galloping - to prevent structural damage, the VIVACE team works towards increasing the amplitude of oscillation and maximizing the hydrokinetic energy converted to mechanical energy in the oscillating cylinder. By introducing PTC, the cylinder's FIM can be enhanced to reach back-to-back VIV and galloping [3-5,7], amplitude-to-diameter ratio exceeding 3 and with no-end to the synchronization range within the capabilities of the Low Turbulence Free Surface Water (LTFSW) Channel at MRELab for $Re<150{,}000$ or the towing tank of the Marine Hydrodynamics Laboratory $Re<500{,}000$. For smooth cylinders, this range falls in flow regimes TrSL2, TrSL3 (Transition in Shear Layer [19,20]). To convert energy to electricity, VIVACE operates under highly added linear viscous damping, and high Reynolds numbers [9]. The harnessing damping ratio used by Lee and Bernitsas [9] was as high as 0.16, compared to a value of 0.0054 for the total damping used by Khalak and Williamson for $2{,}000<Re<12{,}000$ [6].

[1] Professor, also in Mechanical Engineering; and CTO of Vortex Hydro Energy

Wu et al. [18] used Unsteady Reynolds-Averaged Navier Stokes equations (URANS) with the Spalart-Allmaras one-equation turbulence model and solved them numerically for two-dimensional flow over a spring-mounted rigid circular cylinder. The single degree of freedom was transverse to the flow direction and the cylinder axis. In this paper a similar approach is used for multiple cylinders.

Two-dimensional approximation overestimates the hydrodynamic forces on a cylinder. When the cylinder is in VIV or galloping though, the three-dimensional effects are minimal as the correlation length practically spans the entire length of a cylinder in FIM particularly when PTC is applied as straight sand-strips parallel to the cylinder axis [3]. PTC application helps to maintain FIM and limit three-dimensional effects in the lab as well. Two-dimensional URANS simulation of circular-cylinder flows for Re>10,000 is challenging due to the poor ability of URANS to predict properly the motion of the separation point of a cylinder in FIM [18]. Nevertheless, with proper modeling of PTC, URANS simulations exhibit several of the salient features of experiments and can provide complementary flow information, which is difficult to measure experimentally at such high speeds and turbulence levels [18].

In this study, four sets of models with 1/2/3/4 cylinders in tandem are investigated numerically. Simulations are conducted at two Reynolds numbers corresponding to VIV and galloping. Numerical results are compared with experimental MRELab data. The goal is to assess to what extent CFD can be useful in understanding phenomena that are difficult to measure such as VIV to galloping transition, vortex structures, motion of separation point, and pressure distribution.

The physical and numerical models are summarized in Sections 2 and 3, respectively. In Section 4, the results are compared with experiments conducted in the LTFSW Channel of the MRELab for single isolated cylinder [5] and for multiple cylinders [7]. The numerical tool is first tested with a single PTC-cylinder undergoing VIV in Section 4.1. The results for 2/3/4 PTC-cylinders in tandem are presented in Sections 4.2-4.4. Amplitude ratio, frequency ratio, and vortex patterns match well with experimental observations. Conclusions are presented at the end.

2. PHYSICAL MODEL

A simple schematic of the single cylinder VIVACE Converter is shown in Figure 1(a). The elements of this module are: a rigid circular cylinder of diameter D and length L, two end-supporting linear springs each of stiffness $K/2$, and damping of the transmission mechanism and PTO C. The cylinder is placed with its axis in the z-direction, perpendicular to the flow velocity U, which is in the x-direction. The cylinder oscillates in the y-direction, which is perpendicular to its axis (z direction) and the flow velocity (x direction). Four modules of single-cylinder VIVACE Converters in the LTFSW Channel are shown in Figure 1(b). Each cylinder can slide on a rail system to adjust the longitudinal spacing between the four cylinders. Particulars of the four single-cylinder VIVACE Converters are listed in Table 1. Spring stiffness is calibrated by weights and system damping is measured by free decay tests in air.

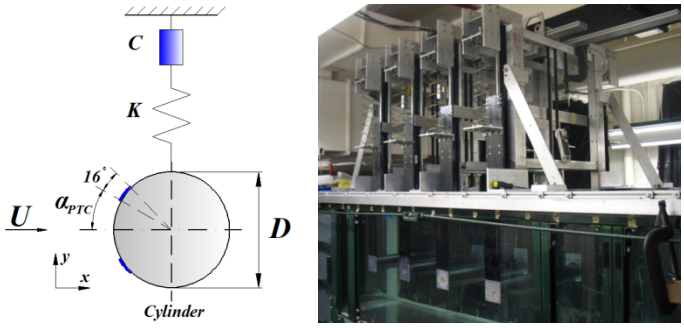

Figure 1. (a) Schematic of single PTC-cylinder physical model; (b) Four-cylinder VIVACE converter in the LTFSW Channel

Table 1. Particulars of the isolated cylinder oscillator and the four single-cylinder oscillators

Parameters	Symbol	Isolated Cylinder	1st Device	2nd Device	3rd Device	4th Device
Diameter [m]	D	0.0889	0.0889	0.0889	0.0889	0.0889
Length [m]	l	0.9144	0.9144	0.9144	0.9144	0.9144
$Mass_{osc}$ [kg]	m	10.75	9.53	9.59	9.51	9.58
Spring const[N/m]	k	1600	744.29	757.41	737.24	747.39
Damping ratio	ζ	0.0099	0.0206	0.0198	0.0172	0.0168
Damping [Ns/m]	C	3.2	3.464	3.382	2.882	2.834
Natural freq. in water	$f_{n,water}$	1.57	1.114	1.121	1.109	1.114
Mass ratio	m^*	1.896	1.681	1.690	1.677	1.689
Added mass [kg]	m_a	5.671	5.671	5.671	5.671	5.671

In the present study, simulations are verified by experimental measurements on the flow induced motion of multiple circular cylinders with PTC in tandem. Passive turbulence control [3-5, 11] has been studied extensively in the MRELab to alter the FIM of multiple cylinders in transverse flow [3-5] culminating in the development of the *PTC-to-FIM Map* for a single circular cylinder [11]. All modeling parameters of PTC are defined in Figure 2. Two roughness strips parallel to the cylinder axis are attached running along the entire length of the cylinder. Strip thickness is equal to the thickness of the boundary layer and affects profoundly FIM. PTC is used in this paper to induce synergetic dynamics of multiple cylinders with large amplitude galloping and dramatic expansion of the synchronization range thus making VIVACE work like a multi-cylinder reciprocating engine. Table 2 shows the details of roughness strip used in the present study. It should be noted that the angle of the PTC (α_{PTC}) for each VIVACE converter systems is different: (a) α_{PTC}=20° for single cylinder; (b) two cylinder cases, α_{PTC} =20° for the 1st cylinder and α_{PTC} =30° for the 2nd cylinder; (c) three PTC-cylinder cases, α_{PTC} =30° for the three cylinders; (d) four cylinder with α_{PTC} =30° PTC for four cylinder cases.

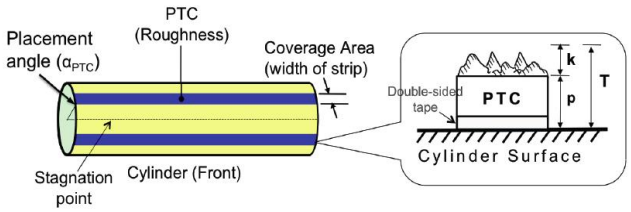

Figure 2. Configuration of sand strips (PTC) along the cylinder

Table 2. Details of roughness strip in PTC (P60)

Angular coverage of strip	[degrees]	16
Sand paper thickness	*P*[mm]	0.587
Average grit height	*k*[mm]	0.260
Total thickness	*T*=*P*+*k* [mm]	0.847

3. NUMERICAL MODEL

3.1. Governing Equations and Turbulence Model

Flow simulations presented in this study are produced by open source CFD tool OpenFOAM, which is composed of C++ libraries solving continuum mechanics problems with a finite-volume discretization method. In addition, code was developed for (a) the dynamics of the four oscillators, (b) dynamic adjustment of the grid near a cylinder as it approaches a boundary. The time-dependent viscous flow solutions are obtained by numerical approximation of the incompressible URANS equations in conjunction with the one-equation Spalart-Allmaras (S-A) turbulence model [15]. The basic equations are:

$$\frac{\partial U_i}{\partial x_i} = 0 \tag{1}$$

$$\frac{\partial U_i}{\partial t} + \frac{\partial}{\partial x_j}\left(U_i U_j\right) = -\frac{1}{\rho}\frac{\partial p}{\partial x_i} + \frac{\partial}{\partial x_j}\left(2\nu S_{ij} - \overline{u_i' u_j'}\right) \tag{2}$$

where ν is the molecular kinematic viscosity and S_{ij} is the mean strain-rate tensor

$$S_{ij} = \frac{1}{2}\left(\frac{\partial U_i}{\partial x_j} + \frac{\partial U_j}{\partial x_i}\right) \tag{3}$$

where U_i is the mean flow velocity vector. The quantity $\rho\overline{u_i' u_j'}$ is known as the Reynolds-stress tensor and is further modeled through the Boussinesq approximation as $\mu_t\left(\frac{\partial U_i}{\partial x_j} + \frac{\partial U_j}{\partial x_i}\right)$, where μ_t is turbulence eddy viscosity.

The S-A model is widely used for turbulence closure and many variants of the model are available in the literature. The original model [16] is employed in this work. The eddy-viscosity coefficient is calculated from the following transport equation

$$\frac{\partial \tilde{\nu}}{\partial t} + u_j \frac{\partial \tilde{\nu}}{\partial x_j} = c_{b1}\tilde{S}\tilde{\nu} - c_{w1} f_w \left(\frac{\tilde{\nu}}{d}\right)^2 + \frac{1}{\sigma}\left\{\frac{\partial}{\partial x_j}\left[\left(\nu + \tilde{\nu}\right)\frac{\partial \tilde{\nu}}{\partial x_j}\right] + c_{b2}\frac{\partial \tilde{\nu}}{\partial x_i}\frac{\partial \tilde{\nu}}{\partial x_i}\right\} \tag{4}$$

where $\tilde{\nu}$ is an intermediate working variable of the turbulence model and the turbulent eddy viscosity μ_t is computed from $\mu_t = \rho\tilde{\nu} f_{v1}$ where $f_{v1} = \frac{\chi^3}{\chi^3 + c_{v1}^3}$ and $\chi = \frac{\tilde{\nu}}{\nu}$.

Additional definitions of functions and constants can be found in the work by Spalart and Allmaras [15]. In this study, the trip terms f_{t1} and f_{t2} are turned off, and at the same time the "Trip-less" initial condition for $\tilde{\nu}$ is used following Travin et al [16]. This approach was proposed by Shur et al [14] to simulate subcritical cylinder flow without a user specified location for transition of flow on the body. The "tripless" initial conditions divide the fluid domain into two regions with different initial values for eddy viscosity. A zero value is applied for the upstream half of cylinder and flow domain, and a nonzero value is used for the downstream half of the cylinder and flow domain. The nonzero value is set at the same level as the molecular eddy viscosity for all the simulations in the present study [18].

A second-order Gauss integration scheme with a linear interpolation for the face-centered value of the unknown is used for the divergence, gradient, and Laplacian terms in the governing equations. The second-order backward Euler method is adopted for time integration. Thus, the numerical discretization scheme gives second order accuracy in space and time. A pressure implicit with splitting of operators (PISO) algorithm is used for solving the momentum and continuity equations together in a segregated way. The body equation-of-motion is solved using a second-order mixed implicit and explicit time integration method.

3.2. Computational Domain and Grid Generation

The computational domain size is different in the stream direction depending on the number of cylinders in tandem. $50D \times 9D$ is used for a single-cylinder, $52.5D \times 9D$ for two cylinders, $55D \times 9D$ for three cylinders, and $57.5D \times 9D$ for four cylinders. Figure 3 shows the computational domain for four PTC-cylinder cases. The entire domain includes five boundaries: inflow, outflow, top and bottom boundary, and the cylinder walls. The distance between the inlet boundary and the center of the1st cylinder, l_{up}, is set at $25D$. The downstream length of the domain, l_{down}, is also set at $25D$. l_{up} and l_{down} are the same regardless of the number of cylinders used in tandem. The distance d between two cylinders is fixed at $2.5D$. The inflow velocity is considered as uniform and constant. At the outflow boundary, a zero gradient condition is specified for velocity as well as v_t and $\tilde{\nu}$. The bottom condition is defined as a wall boundary to match the experimental conditions. In the present numerical study, the free surface is simplified by modeling it as a wall. A moving wall boundary condition is applied for the cylinder surface when the cylinders are in flow induced motion. In addition, similar to the "Trip-less" initial condition for the one-cylinder simulation [18], the fluid domain is divided into two regions: (a) from the upstream inlet to the center of the 1st cylinder, a zero value is applied for the eddy viscosity, and a nonzero value is used for the downstream-half of the 1st cylinder through the downstream cylinders to the

outlet of the flow domain. The nonzero value is set equal to the molecular eddy viscosity for all simulations.

In summary, the body and channel boundary conditions in the numerical model match the physical model conditions as described in Section 2 with the exception of the free surface, which is modeled by a wall.

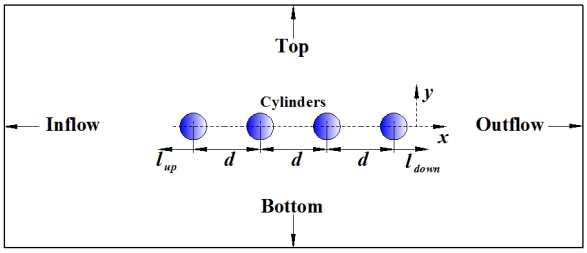

Figure 3. Computational domain for 4 cylinders

Two-dimensional, structured, computational grids were generated for all cases using the Gambit grid-generating software. The computational domain in the vicinity of each cylinder is a $2D \times 2D$ square where the grid density for the near-wall region is enhanced to solve for high resolution in flow properties. For the cylinder with PTC, due to the specifically modified surface geometry, a wall function type boundary condition is used to account for the effect of surface roughness. Due to the nature of the wall-function for the roughness model used in this study, the near-wall grid spacing was selected to produce a y+ between 30-70, depending on the Reynolds number. In order to determine the overall grid resolution to achieve a convergent and accurate solution in reasonable computational-time, three different grid densities were considered in earlier work. A grid sensitivity study was conducted and the medium grid was successfully used to simulate one cylinder with PTC in FIM [18]. In this paper, the medium grid resolution for the multiple PTC-cylinders was selected as well. A close-up of the medium grid for the case of four PTC-cylinders is shown in Figure 4.

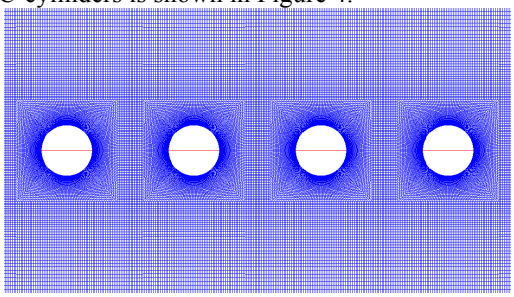

Figure 4. Close-up of the medium grid for 4 PTC-cylinders

4. RESULTS AND DISCUSSION

Simulations are carried out at two Reynolds numbers for PTC-cylinders in each case. For a single cylinder Re=60,000 and Re=90,000 are used. For 2,3, and 4 cylinders Re=62,049 and Re=90,254 are used. The results are presented in Figure 5 and summarized in Table 3. Comparisons are made with experiments conducted in the LTFSW Channel of the MRELab. In both the experiments and the simulations the amplitude, A_{peak}, of each cylinder is calculated by averaging the absolute values of the 60 highest positive and negative peaks. The frequency of oscillation for each cylinder is processed using Fast Fourier Transform. The dominant frequency of oscillation is found and non-dimensionalized by the corresponding system natural frequency in water, $f_{n,water}$.

Table 3. Results of isolated PTC-cylinder and multiple PTC-cylinder cases

U(m/s)	*Re*	Models		Amplitude ratio[A_{peak}/D]				Frequency ratio[$f_{osc}/f_{n,water}$]			
				1st	2nd	3rd	4th	1st	2nd	3rd	4th
0.76	60,000	Single cylinder	CFD	1.63				1.07			
			Experiment	1.2				0.992			
0.79	62,049	Two cylinders	CFD	1.76	1.22			1.02	1.07		
			Experiment	1.23	1.19			1.15	1.01		
		Three cylinders	CFD	1.91	1.33	1.12		1.08	1.08	1.09	
			Experiment	1.16	1.27	1.14		1.15	1.03	1.02	
		Four cylinders	CFD	1.85	1.39	1.25	1.39	1.07	1.08	1.09	1.09
			Experiment	1.13	1.21	1.14	1.07	1.18	0.99	1.00	1.00
1.157	90,000	Single cylinder	CFD	1.87				1.09			
			Experiment	2.41				0.992			
1.16	90,254	2 cylinders	CFD	1.77	2.44			1.07	1.09		
			Experiment	2.56	2.05			1.10	1.02		
		3 cylinders	CFD	2.49	1.83	1.50		1.04	1.07	1.08	
			Experiment	2.29	1.78	2.51		1.08	1.09	1.04	
		4 cylinders	CFD	2.49	1.52	1.45	1.27	1.05	0.96	1.09	1.12
			Experiment	2.31	1.67	2.50	1.82	1.07	1.07	1.03	1.03

For the cases of Re=60,000 for a single cylinder and Re=62,049 for multiple cylinders, as shown in Table 3 and Figure 5, the amplitude ratio of the 1st cylinder of all models is over-predicted by simulation compared with experimental data. The maximum amplitude of $1.91D$ is obtained in the CFD results for the 3-cylinder case. The amplitudes of the cylinders located downstream are in good agreement with experimental

data except for the 4-cylinder case, which shows a 20% over-prediction by CFD. For Re=90,254, higher amplitudes are reached, especially for the 3- and 4-cylinder sets where A_{peak}=2.49D is obtained by the CFD simulations.

The frequency ratio shown in Figure 5 and Table 3 is in good agreement between experiments and simulations. The oscillation frequency is very close to the corresponding system natural frequency.

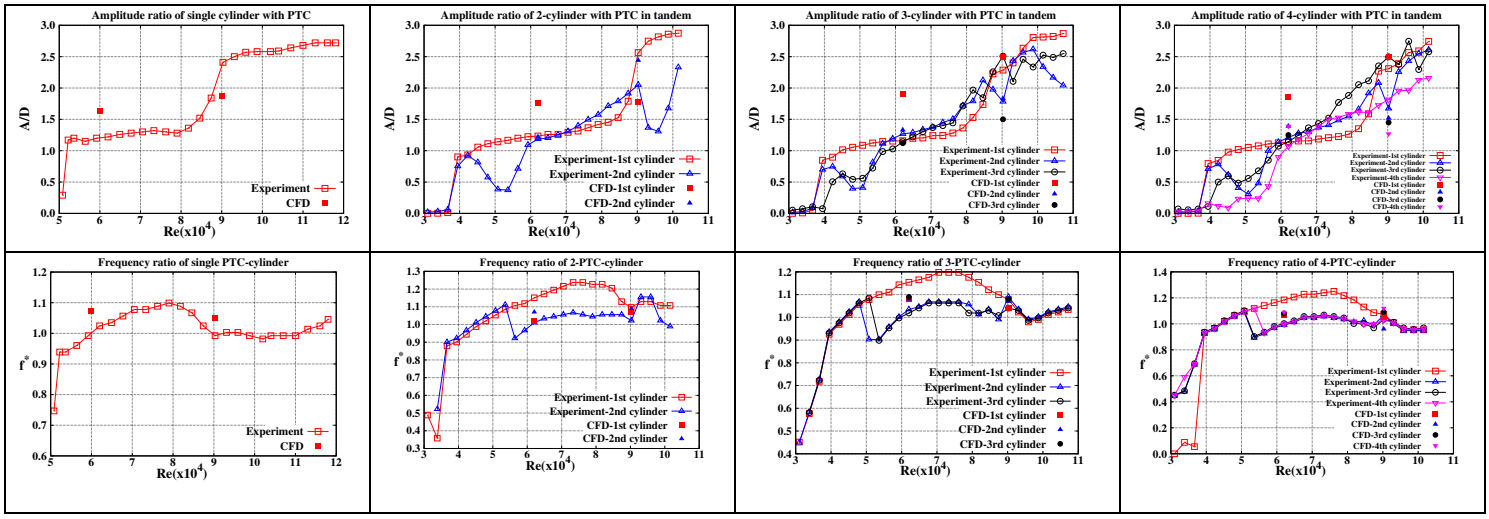

Figure 5. Comparison of amplitude and frequency ratios between CFD and experiments: Single cylinder [5], multiple cylinders [7].

4.1. Flow-Induced Motion of Single PTC-Cylinder

The simulation results for the single PTC-cylinder are presented in Figures 6-9. At *Re*=60,000, the cylinder is in its VIV upper branch. As shown in Figure 6, the vortex pattern P is observed on the upper side of the cylinder and S on the lower side where P stands for "pair" and S for "single" [17]. Amplitude and frequency response (Fig. 7) are closely related to the vortex dynamics and wake pattern. The amplitude of the cylinder is nearly uniform throughout the time history and amplitude ratio of 1.63D is obtained in the simulation. In addition, oscillation frequency of 1.07$f_{n,water}$ is reached, that is 7% higher than the natural frequency in water.

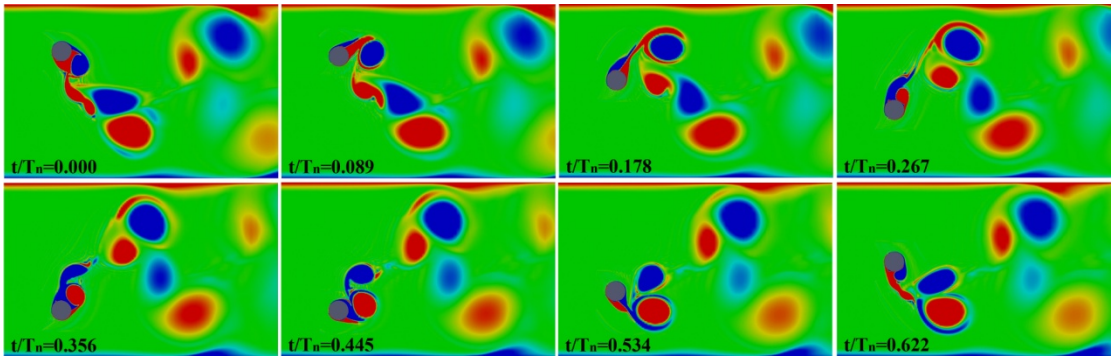

Figure 6. Wake structure for single cylinder; *Re*=60,000

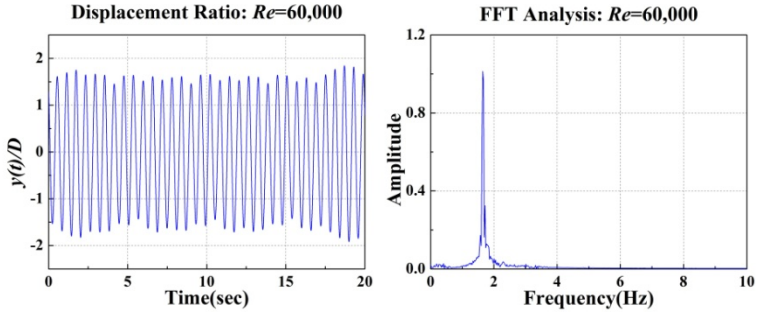

Figure 7. Displacement and FFT for single cylinder; *Re*=60,000

For *Re*=90,000 (Fig. 8), eight vortices are observed per cycle. The vortex structure is P+2S on each side of the cylinder. This is the vortex wake periodicity is faster than that of the motion. This is the case in transition from VIV to galloping where both mechanisms of FIM coexist. At the end of transition to fully developed galloping, the vortex patterns do not drive the FIM. Instead, the galloping mechanism based on instability and synchronization of FIM with the shear layer motion drives the cylinder motion. This observation is in agreement with the perfectly periodic motion of the cylinder (Fig. 9). The amplitude of oscillation is 1.87*D* and the frequency is $1.09f_{n,water}$. More information on the FIM of single cylinder with PTC can be found in earlier work [18].

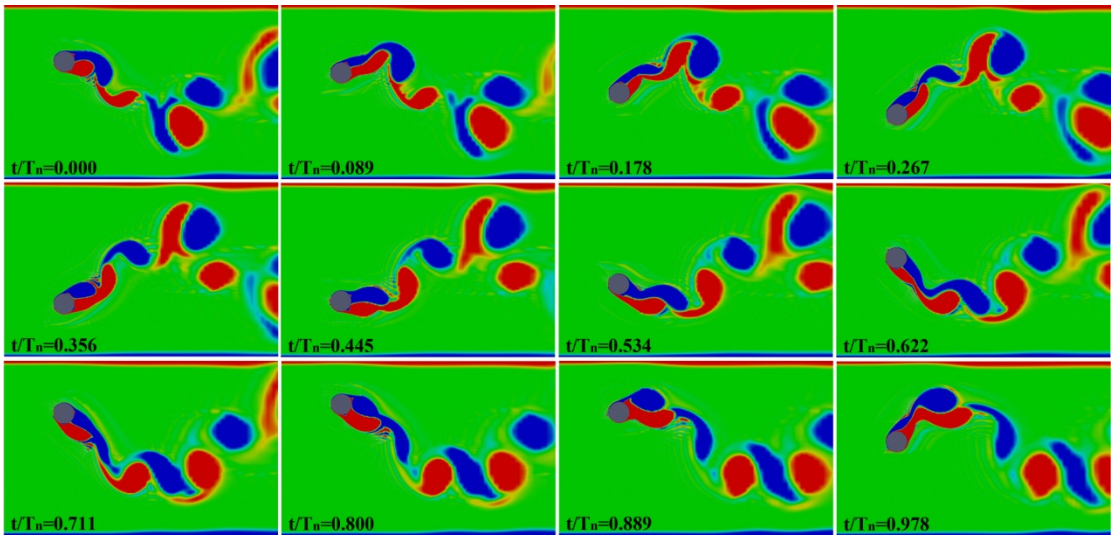

Figure 8. Wake vortex-structure for single cylinder; *Re*=90,000

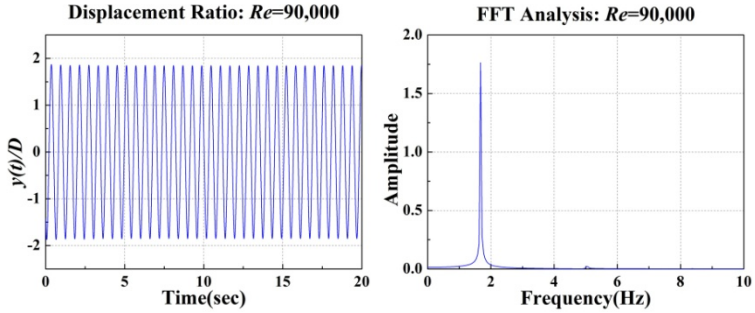

Figure 9. Displacement and FFT for single cylinder; *Re*=90,000

4.2. Flow-Induced Motion of Two PTC-Cylinders in Tandem

The wake vortex-structure, displacement, and frequency response for two PTC-cylinders are illustrated in Figures 10-13. For *Re*=62,049, both cylinders generate 2P vortex patterns as shown in Figure 10. The upstream vortices directly and closely interact with the downstream cylinder. The motion of the 1st cylinder shows a periodic pattern with small variation. The motion of the 2nd cylinder exhibits nearly a beating phenomenon resulting in small oscillations in certain cycles. Two peaks appear in the FFT analysis for the 2nd cylinder, as shown in Figure 11. The first peak corresponds to the same frequency as the peak of the FFT of the 1st cylinder. The reason for the small displacement in those cycles is that the vortex development of 2nd cylinder is weakened by the shed vortices from 1st cylinder. Specifically, when a shed vortex from the first cylinder reaches the second cylinder, it absorbs the vorticity of the same sign (same side) attached to the second cylinder, thus, eliminating the partially developed vortex on the second cylinder.

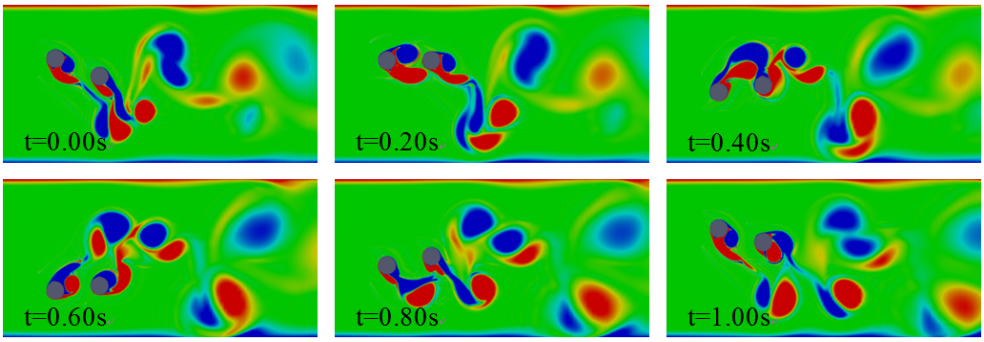

Figure 10. Wake-vortex structure for two cylinders in tandem; *Re*=62,049

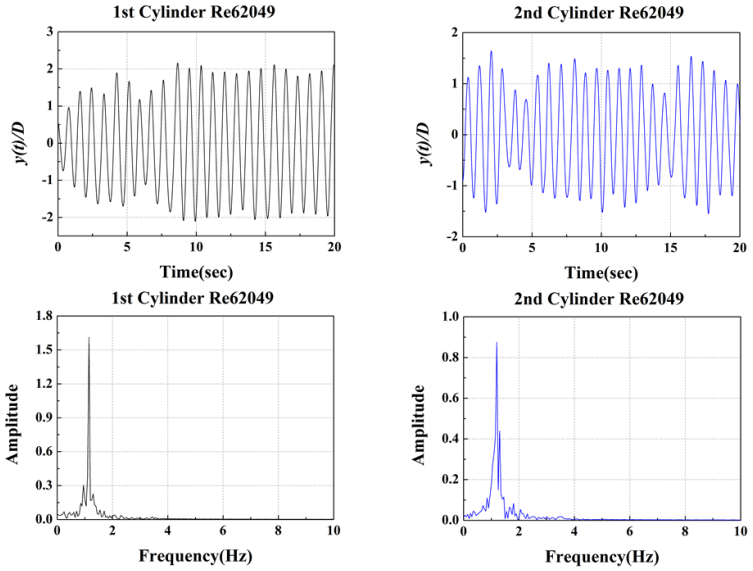

Figure 11. Displacement and FFT for two cylinders in tandem; *Re*=62,049

For *Re*=90,254, both cylinders shed vortices in 2P+2S mode (Fig. 12). Occasionally, in the first cylinder shedding, one more vortex is shed in the upward travel; that is, there is cycle-to-cycle variation in vortex shedding. For the 2nd cylinder, the vortices are disrupted and modified by the vortices shed by the upstream cylinder. The maximum displacement of the 2nd cylinder reaches 2.44*D*, as shown in the displacement ratio curves in Figure 13. That is, the response of the 2nd cylinder is higher than the 1st cylinder for this Reynolds number which is close to galloping.

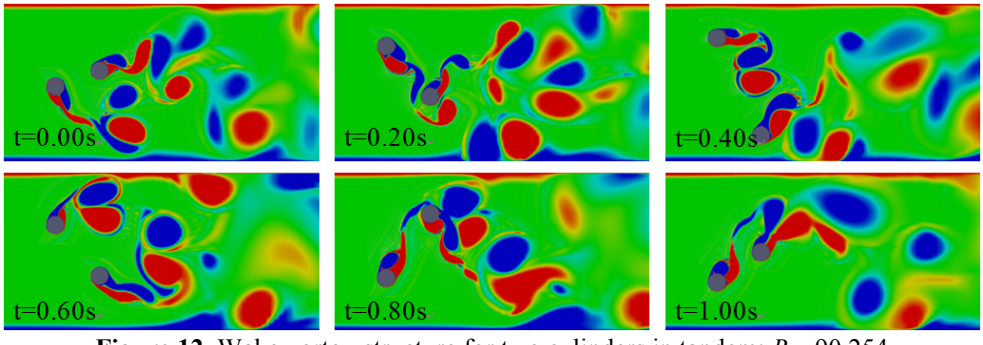

Figure 12. Wake vortex-structure for two cylinders in tandem; *Re*=90,254

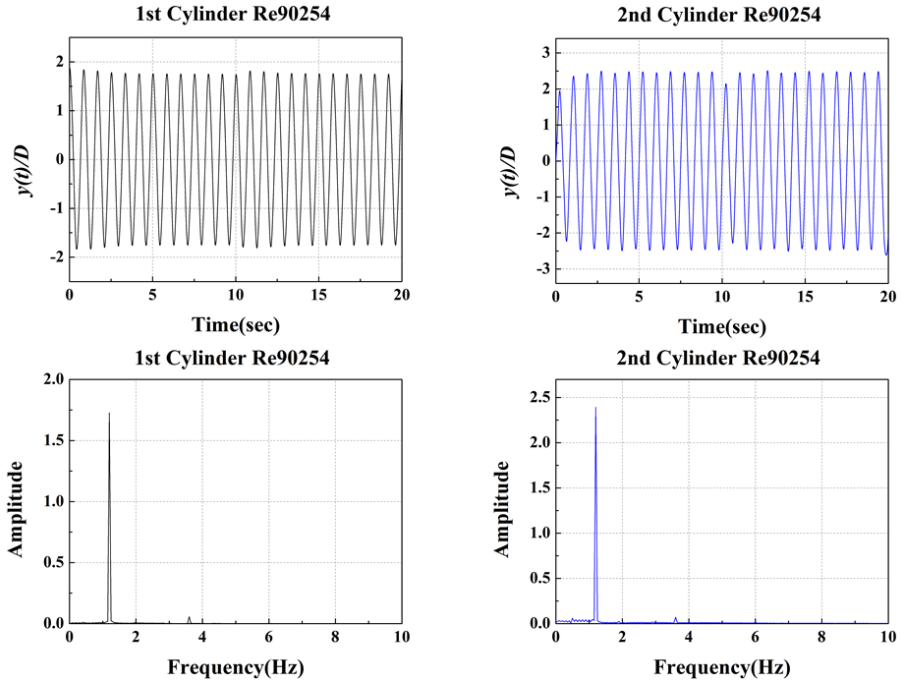

Figure 13. Displacement and FFT for two cylinders in tandem; *Re*=90,254

4.3. Flow-Induced Motion of Three PTC-Cylinders in Tandem

For the three-cylinder cases, the motions of the downstream cylinders are strongly influenced by the vortices shed by the 1st cylinder. For *Re*=62,094, as presented in Figure 14, the vortex pattern of the 1st cylinder is 2P+2S and different from that of the 1st cylinder for the two-cylinder case. The vortices developed by the 2nd and 3rd cylinders are taken away and absorbed by the upstream vortices. It is hard to identify the vortex pattern for the 2nd and 3rd cylinders. Figure 15 shows the displacement and frequency response of all three cylinders. The amplitude is higher for the upstream cylinder. The frequencies of the three cylinders are close to each other.

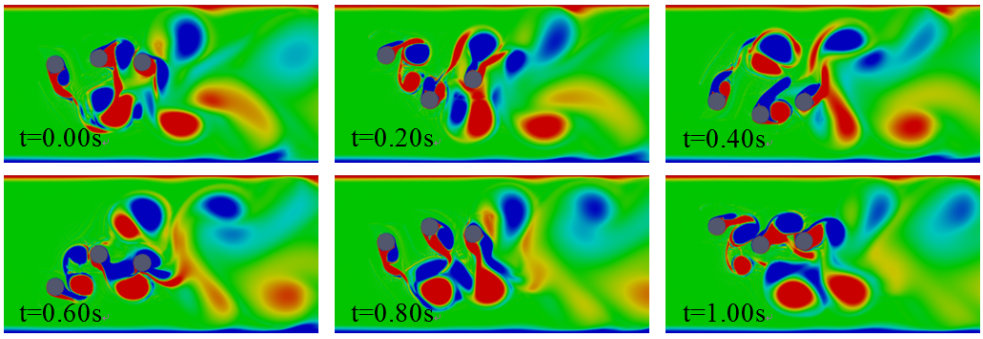

Figure 14. Wake vortex-structure for the three cylinders in tandem; *Re*=62,049

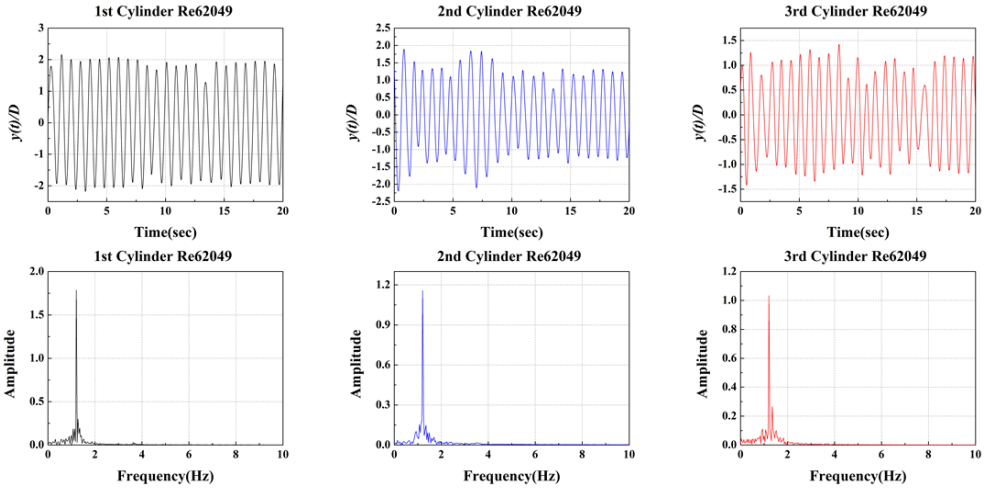

Figure 15. Displacement and FFT for three cylinders in tandem; *Re*=62,049

In Figure 16, the vortex pattern of three PTC-cylinders for *Re*=90,254 is plotted. Eight vortices are shed by the 1st cylinder in a 2P+4S vortex-structure. The vortex pattern is not clear for the 2nd and 3rd cylinders. It should be noted that the 2nd cylinder follows the 1st cylinder and its vortex shedding is disturbed by upstream vortices. Thus, the displacement of the 2nd cylinder is influenced and small amplitude in some cycles is obtained, as shown in Figure 17. Amplitude ratio of A_{peaks}/D=2.49 is reached for the 1st cylinder.

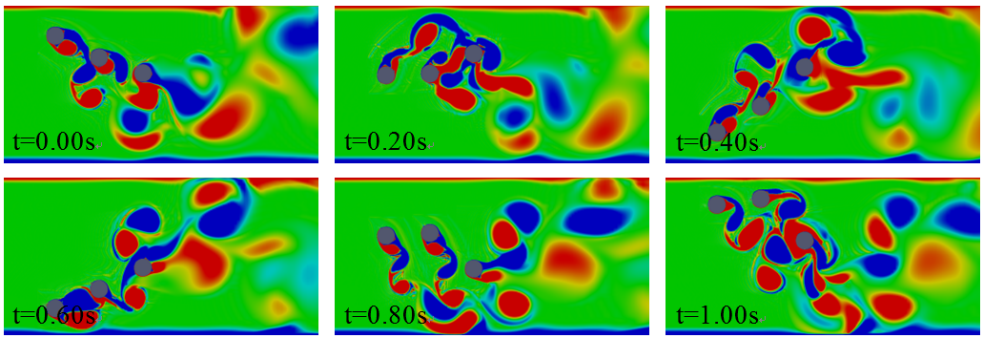

Figure 16. Wake vortex-structure for three cylinders in tandem; *Re*=90,254

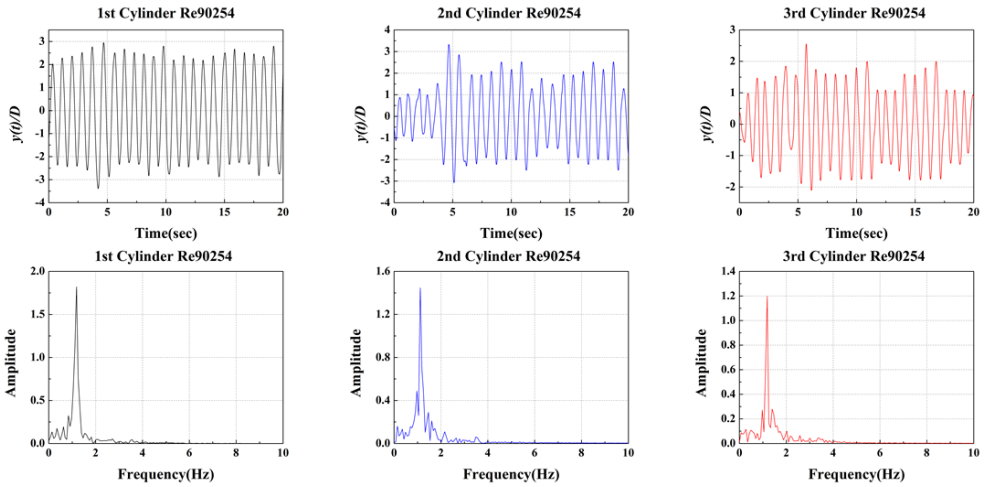

Figure 17. Displacement and FFT for three cylinders in tandem; *Re*=90,254

4.4. Flow-Induced Motion of Four PTC-Cylinders in Tandem

For *Re*=62,049, the presence of the other three cylinders practically does not affect the oscillations of the 1st cylinder. In this case, the 1st cylinder experiences VIV and the 2P vortex pattern as observed in Figure 18. It is worthwhile to note that significant phase difference exists between two adjacent cylinders. There is a nearly 180° phase lag between the 3rd and 4th cylinders. The shear layers of the downstream cylinders are significantly affected by the wake of the upstream cylinders. The oscillation frequencies are very close for all four cylinders as can be seen in Figure 19 and Table 3. The amplitude is about 1.85*D* for the 1st cylinder and decreases gradually from the first to the last cylinder.

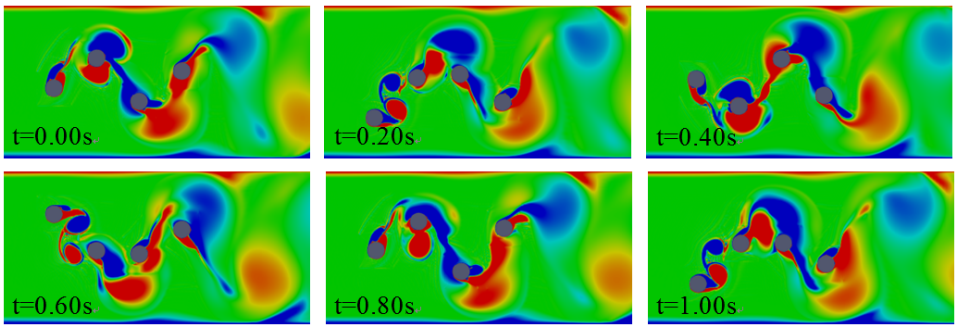

Figure 18. Wake vortex-structure for four cylinders in tandem; *Re*=62,049

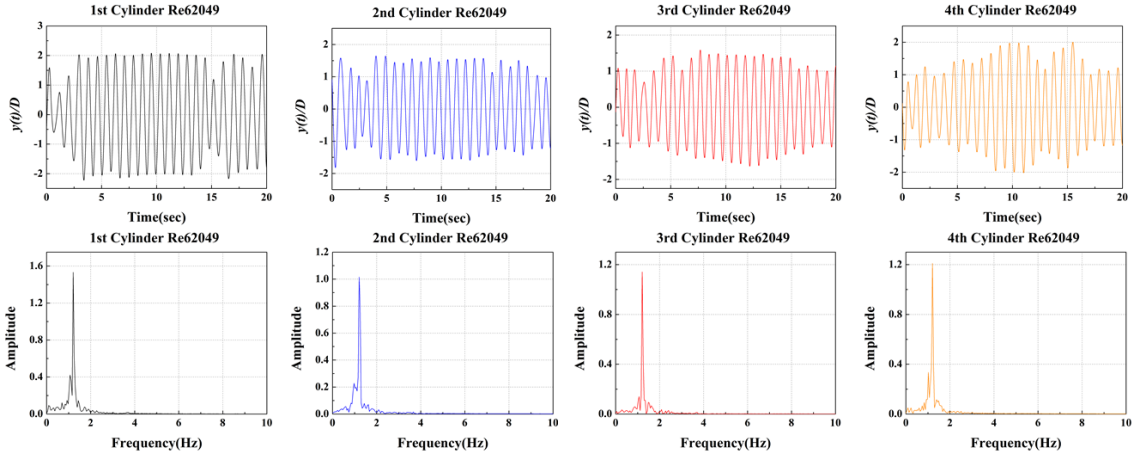

Figure 19. Displacement and FFT for four cylinders in tandem; *Re*=62,049

As shown in Figure 20 for *Re*=90,254, when the 1st cylinder moves down from the point of maximum displacement, a pair (P) of vortices sheds from the cylinder, followed closely by a single vortex (S). The same is observed on the other side of the cylinder. Thus, the vortex model is 2P+2S for the 1st cylinder. Amplitude ratio A_{peaks}/D=2.49 is achieved by the 1st cylinder. The amplitudes of cylinders 2-4 are high and exhibit multiple frequencies as shown in the FFTs in Figure 21.

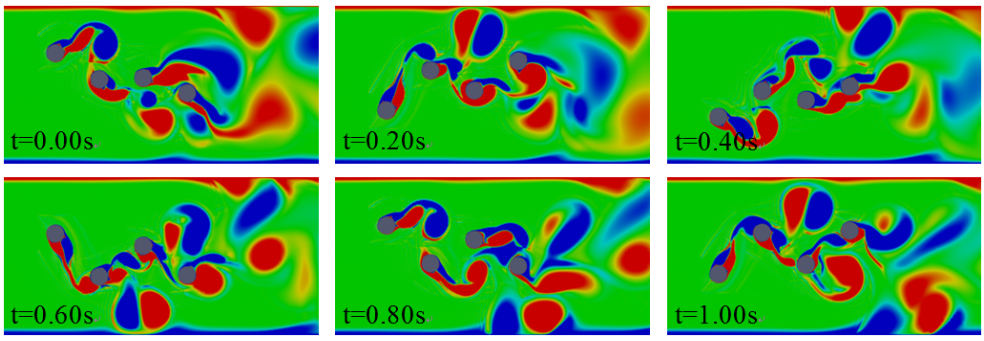

Figure 20. Wake vortex-structure for four cylinders in tandem; *Re*=90,254

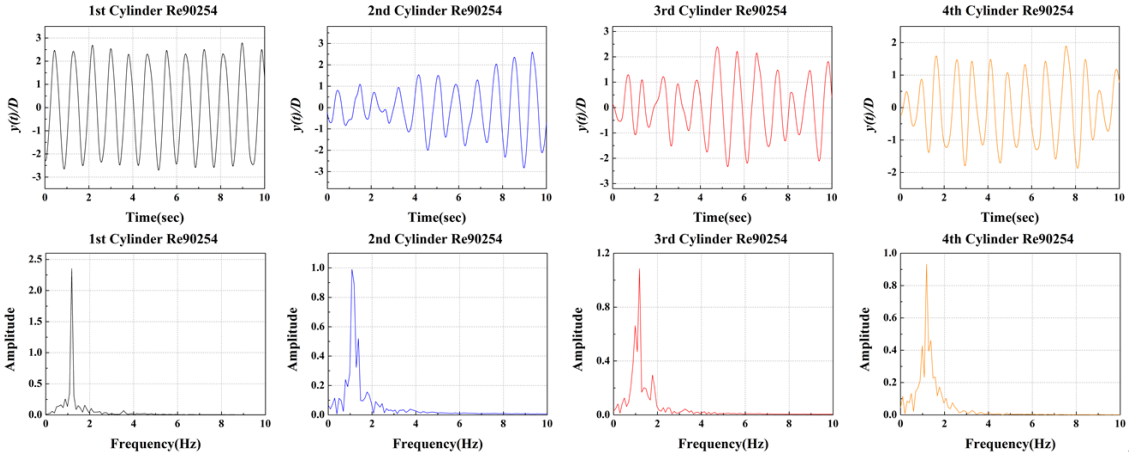

Figure 21. Displacement and FFT for four cylinders in tandem; *Re*=90,254

5. CONCLUSIONS

(1) A 2D-URANS code based on OpenFOAM was developed to study numerically FIM of multiple circular cylinders with passive turbulence control. PTC has made it possible to have good agreement with experiments as was proven in the past for a single PTC-cylinder.

(2) Four models with 1/2/3/4 cylinders were investigated for two Reynolds numbers around 60,000 and 90,000. For the 1st cylinder, Re≅60,000 corresponds to VIV while Re≅ 90,000 is in the VIV to galloping transition range.

(3) 2-D URANS for multiple PTC-cylinders generates CFD simulation captures salient features of the flow and cylinder response. For the first cylinder, A_{peaks}/D≅1.7-1.9 is obtained at *Re*=62,049; $A_{peaks}/D \cong 2.5$ is reached for *Re*=90,254. Response frequency is in good agreement with experiments.

(4) Vortex structures show significant variation in different flow regimes following experimental observations.

(5) At *Re*=90,254, up to 8 vortices per cycle are generated showing that the driving force in galloping is not vortex shedding but the shear layer motion.

Comparison with experiments shows that the developed CFD tool can be useful in understanding the behavior of multiple cylinders in VIV and galloping. Multiple-cylinder FIM though is very complex and extensive study is required to draw conclusions about specific configurations. The computational time is high, on the order of 500 hours one-processor equivalent for about 20 seconds of real time simulation.

NOMENCLATURE

A_{peaks}	Mean amplitude of the peaks
K	Spring constant
D	Cylinder diameter
P	Thickness of sand paper
T	Total thickness of PTC
U	Mean flow velocity
$U_{r,water}=U/(f_{n,water}D)$	Reduced velocity in water
C	Structural damping
f_{osc}	Oscillating frequency of cylinder
$f_{n,water}=\sqrt{K/(m+m_a}/2\pi$	System natural frequency in water
k	Average height of sand grits
m_d	displaced fluid mass
$m_a= C_a m_d$	Added mass
m_o	Oscillating mass of system
$m^*= m_o/(m_d)$	Mass ratio
p	pressure
$y(t)$	Displacement of cylinder
$y+$	Nondimensional first grid spacing
α_{PTC}	PTC placement angle
$\zeta_{harn}= c_{harn}/(2\sqrt{m_o K})$	Damping ratio for harnessing
ν	Kinematic molecular viscosity
μ_t	Turbulent eddy viscosity
$\tilde{\nu}$	Intermediate working variable

ACKNOWLEDGMENTS

The following support is gratefully acknowledged: (a) DOE contract DE-EE0003644 to Vortex Hydro Energy with subcontract to the University of Michigan. (b) NSF-SBIR grant to Vortex Hydro Energy and the University of Michigan award # IIP-0810426. (c) China Scholarship Council and the Ph.D. Program Foundation of Ministry of Education of China (Grant No. 20120191130003) for Lin Ding.

REFERENCES

1. Bernitsas, M. M., and Raghavan, K., "Reduction/ Suppression of VIV of Circular Cylinders through Roughness Distribution at 8×10^3<Re<1.5×10^5," Proceedings, OMAE-2008 Conf., Paper #58024, Estoril, Portugal, June, 2008.
2. Bernitsas M.M., Ben-Simon Y., Raghavan K., Garcia E. M. H., "The VIVACE Converter: Model Tests at Reynolds Numbers Around 10^5", OMAE 2006; and Journal of Offshore Mechanics and Arctic Engineering, ASME Trans., Feb. 2009, Vol. 131, No. 1, pp. 1-13.

3. Chang, C.C. and M.M. Bernitsas, "Design of VIVACE Converter using PTC", Proceedings of the 30th OMAE 2011 Rotterdam, The Netherlands, June 2011.
4. Chang, C.C., R.A. Kumar, and M.M. Bernitsas, "VIV and Galloping of Single Circular Cylinder with Surface Roughness at $3.0 \bullet 10^4 < Re < 1.2 \bullet 10^5$", Ocean Engineering, 2011. 38(16): p. 1713-1732.
5. Chang, C.C., "Hydrokinetic Energy Harnessing by Enhancement of Flow Induced Motion Using Passive Turbulence Control," Ph.D. Dissertation, Dept. of NA&ME, University of Michigan, 2010.
6. Khalak, A. and C.H.K. Williamson, "Dynamics of a Hydroelastic Cylinder with Very Low Mass and Damping", Journal of Fluids and Structures, 1996. 10(5): p. 455-472.
7. Kim E.S., Bernitsas M.M., Kumar, A.R., (2011), "Multi-Cylinder Flow Induced Motions: Enhancement by Passive Turbulence Control at 28,000<Re<120,000," OMAE 2011, paper #49405, Rotterdam, The Netherlands; Journal of Offshore Mechanics and Arctic Engineering, ASME Transactions, Vol.135, No. 1, Feb. 2013.
8. Lee J.H., Chang C. C., Xiros N., and Bernitsas M. M., " Integrated Power Take Off and Virtual Oscillator System for the VIVACE Converter: Vck System Identification", Proceedings ASME Intern. Engineering Congress and Exposition, Paper #, IMECE2009-11430, Lake Buena Vista, FL, Nov. 13-19, 2009.
9. Lee J.H. and Bernitsas M. M., "High-Damping, High-Reynolds VIV Tests for Energy Harnessing Using the VIVACE Converter", Ocean Engineering, Vol.38, #16, Nov. 2011, pp.1697-1712.
10. Lee J.H., Xiros N., and Bernitsas M. M., "Virtual Damper-Spring System for VIV Experiments and Hydrokinetic Energy Conversion", Ocean Engineering, Vol.38, #5-6, April. 2011, pp.732-747.
11. Park, H., M.M. Bernitsas, and R.A. Kumar, "Selective Roughness in the Boundary Layer to Suppress Flow-Induced Motions of Circular Cylinder at $30,000 < Re < 120,000$", Journal of Offshore Mechanics and Arctic Engineering, 2012. 134(4): p. 041801.
12. Raghavan, K., and Bernitsas, M. M., "Enhancement of High Damping VIV through Roughness Distribution for Energy Harnessing at $8 \times 10^3 < Re < 1.5 \times 10^5$," Proceedings of the 27th OMAE'08 Conf., Paper #58042, Estoril, Portugal, June 15-20, 2008.
13. Raghavan, K., Bernitsas, M. M. (2010), "Experimental Investigation of Reynolds Number Effect on Vortex Induced Vibration of Rigid Cylinder on Elastic Supports," Ocean Engineering, Vol.38, #5-6, April 2011, pp.719-731.
14. Shur, M., Sparlart, P., Strelets, M., Travin, A., "Navier-Stokes Simulation of Shedding Turbulent Flow Past a Circular Cylinder and a Cylinder with Backward Splitter Plate", Computational Fluid Dynamics '96, editors J.A. Desideri, et al.1996. 676-682.
15. Spalart, P.R. and S.R. Allmaras, "A One-Equation Turbulence Model Dynamic Flows", Recherche Aerospatiale, 1994(1): p. 5-21.
16. Travin, A., Shur, M., Strelets, M., Spalart, P., "Detached-Eddy Simulations Past a Circular Cylinder", Flow Turbulence and Combustion, 2000. 63(1-4): p. 293-313.
17. Williamson, C.H.K., Roshko, A. "Vortex Formation in the Wake of an Oscillating Cylinder," Journal of Fluids and Structures 2 (1988): 355-381.
18. Wu, W., Bernitsas M.M., Maki, K.J., "URANS Simulation vs. Experimental Measurements of Flow Induced Motion of Circular Cylinder with Passive Turbulence Control at $30,000 < Re < 120,000$," OMAE-2011, paper #50293, Rotterdam, The Netherlands; Journal of Offshore Mechanics and Arctic Engineering, ASME Transactions, in press 2013.
19. Zdravkovich, M.M., "Flow Around Circular Cylinders Vol. 1: Fundamentals", 1997, Oxford University Press.
20. Zdravkovich, M.M., "Flow Around Circular Cylinders Vol. 2: Applications", 1997, Oxford University Press.